Some dynamical aspects of the water drop formation in a leaky faucet

M. S. F. da Rocha, J. C. Sartorelli,* W. M. Gonçalves, and R. D. Pinto
Instituto de Física, Universidade de São Paulo, Caixa Postal 66318, CEP 05389-970, São Paulo, Brazil
(Received 29 April 1996)

We studied the drop formation in a dripping faucet at room temperature by the direct observation of the drop growing which was recorded with a VHS camera, from a drop rate of $f=0.24$ drop/s up to $f\approx 10$ drops/s, approximately, simultaneously with the measurement of the interdrops time intervals. It is shown that the appearance of satellites drops the number of them and its size depends on the drop rate. We observed that the formation of a drop can be seen as a mean elastic motion followed by a plastic motion. [S1063-651X(96)00409-6]

PACS number(s): 05.45.+b, 47.52.+j

I. INTRODUCTION

Complex dynamical behavior has been observed in a leaky faucet, such as periodic and nonperiodic attractors, and period doubling by Martien *et al.* [1,2], Yépez *et al.* [3], Cahalan *et al.* [4], Wu and Schelly [5], Dreyer *et al.* [6], and Sartorelli *et al.* [7]. Tangent intermittencies can be found in Refs. [4,7], quasiperiodicity and boundary crisis in Ref. [7], Hopf bifurcation in [8] and long range anticorrelation and non-Gaussian behavior in [9]. In all these experiments the characterization of the dynamical behavior was done indirectly by measuring the time delay between drops. Experimental studies of water drops or droplet formation, and other viscous liquids as glycerol, using high speed cameras as well as numerical simulations can be found in Refs. [10–15].

Some experimental data were simulated by Martien *et al.* [1,2], supposing that in the nipple faucet the growing drop oscillates according to the mass-spring model

$$\frac{d}{dt}\left(m\frac{dy}{dt}\right)=mg-ky-b\frac{dy}{dt}, \tag{1}$$

where y is the forming drop position. The behavior of the solutions depends on the spring constant k, the friction constant b, $m(t)$, and g. With a decreasing frequency, the drop mass increases linearly with time until it reaches a critical point and breaks away imposing the initial conditions for the next drop. Sánches-Ortiz and Salas-Brito [16] improved Shaw's model supposing that the mass of the falling drop also depends on the current value of the hanged water column and they found evidences of boundary crisis and intermittence. Oliveira and Penna [17] adopting an Ising-like model simulated some dynamic evolution of a growing drop.

We studied the drop formation by the direct observation of the drop growing which was recorded with a VHS camera, from a drop rate of $f=0.12$ drop/s up to $f\approx 10$ drops/s, approximately, simultaneously with the measurement of the interdrop time intervals.

II. EXPERIMENTAL APPARATUS

The experimental apparatus consists of three water reservoirs of 50 liters each. The top reservoir is the source reservoir for the middle one, shown in Fig. 1, and a collector reservoir. The source and the middle reservoirs are coated with a thermal insulator material. The drop rate can be established in two ways: (a) fixing the water level of the middle reservoir with a carburetor valve and controlling the opening of a needle valve driven by a step motor; (b) fixing the overture of the faucet and turning off the water supply to the middle reservoir and letting the water level decrease naturally so the drop rate.

The detection system consists of a He-Ne laser and a photodiode. The induced pulse in the photodiode by the drop passage through the laser beam is detected via a microcomputer parallel port. The pulses are sketched in Fig. 2.

When each drop starts (ends) to cross the laser beam a logic level change in the parallel port is detected, a count variable c is reset and gated. The resolution of the driver software is in the range $3-10$ μs and the minimum detectable time interval is less than 45 μs, which allowed us to measure not only the time between drops (t_n) but the crossing time (δt_n) of the drop through the laser beam. In this case, t_n corresponds to the measurement of a coordinate of the nth drop relative to the $(n+1)$th drop, while δt_n, is a

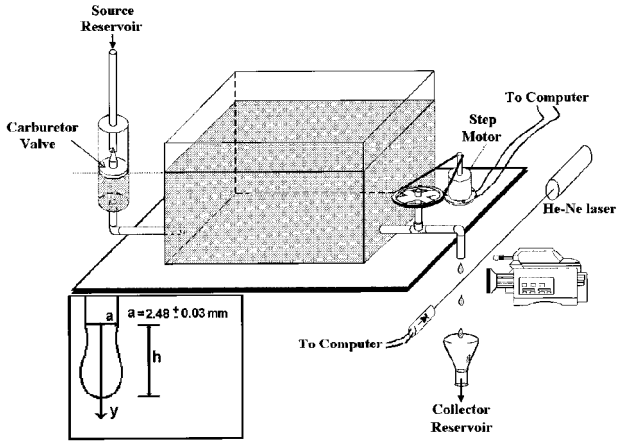

FIG. 1. Diagram of the experimental apparatus. The inset shows a sketch of a drop in formation with the definitions of the variables.

*Electronic address: sartorelli@if.usp.br

 © 1996 The American Physical Society

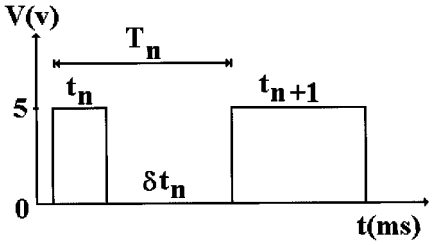

FIG. 2. Pulses induced in the parallel port by the drop passage through the laser beam.

measurement of an absolute coordinate of the nth drop. In some cases we have measured the total time delay $T_n = t_n + \delta t_n$. Therefore three kinds of return maps can be constructed, t_{n+1} vs t_n and δt_{n+1} vs δt_n and T_{n+1} vs T_n to typify the same motion.

The mean time drop formation is given by

$$\langle t_f \rangle = \langle t \rangle + \langle \delta t \rangle = \langle T \rangle \tag{2}$$

and we define the mean drop rate as $f = 1/\langle t_f \rangle$.

To search for a particular attractor, by varying the drop rate as described above, we can construct first return maps on the computer screen in a real time data acquisition mode.

The drop formation was recorded with a VHS camera (simultaneously to the time data acquisition), with the shutter speeds in the range $1/250 - 1/8000$ s^{-1}. Depending on the drop rate, the corresponding black and white images were digitized at the rate of 15, 30, or 60 frames/s and stored as BMP (bit map) format files and compressed in a VSF (video sequence file) format file. From each BMP frame the drop profile was obtained by detecting the variation of the gray level at the border of the drop. A software in C language was developed to obtain the time evolution of the volume and of the center of mass position (relative to the faucet nipple) from the two-dimensional images of the drop, supposing that the drops have a vertical symmetry axis. The video images had a resolution of 480×320 pixels, and for the conversion from pixels to millimeter we used the diameter ($d = 4.96 \pm 0.005$ mm) of the nipple faucet as a reference, therefore the estimated error varies from 2 up to 8% for the center of mass, and from 6 up to 12% for the errors in the volume.

III. RESULTS AND DISCUSSION

In Fig. 3(a) are shown the images of a drop formation at $f = 1.49$ drops/s. Despite the rate of digitalization of 15 frames/s, an oscillatory character of motion can be seen. In Fig. 3(b) are shown the images of two successive drops at $f = 6.21$ drops/s accomplished by the formation of small secondary or satellites drops. We have observed that the occurrence of satellites drops and their number depends on the drop rate. Below $f \approx 2.6$ drops/s for every parent drop there is just one satellite drop and above $f \approx 10$ drops/s we did not observe the formation of any satellite drop. In the range $2.6 < f < 10$ drops/s, for some drop rates no satellites drops are created while for other drop rates the appearance of the satellites and the number of them is intermittent. Sometimes the satellite drop is shot laterally, as shown in Fig. 3(c), therefore it does not cross the laser beam and there is no detection.

As in the low drop rate side ($f < 2.6$ drops/s) we have observed just one satellite drop for every parent drop and we measured the time delay (T_{Dd}) parent satellite as a function of the drop rate, as shown in Fig. 4. It also shows the crossing time of the satellite drops through the laser beam. The time delay increases almost linearly in the range ($0.1 - 3$ drops/s) while the crossing time reaches a plateau of $\delta t \approx 2.4$ ms at $f \approx 0.7$ drops/s.

In Fig. 5 are shown three return maps T_{n+1} vs T_n for $f = 0.24$, 1.04, 1.49 drops/s, together the respective temporal series T_n vs n. The first two regimes are periodic and the last one is a nonperiodic one. As for each parent there is a satellite drop; we added the data of the satellite drop to its respective data parent drop to construct these return maps. If we had not adopted this procedure we would have in Fig. 5(b) a period-two attractor pattern.

In Fig. 6 is shown the volume time evolution, where we included the data for $f \approx 10.0$ drops/s. We observed the same quasilinear (linear plus a small oscillatory behavior) volume time evolution for periodic as well as for nonperiodic motion, therefore we can write for the time evolution of the mean volume

$$\langle V \rangle \approx V_o + \langle \Phi \rangle t, \tag{3}$$

where $\langle \Phi \rangle$ is the mean water flux.

The nonlinear character of the dynamics can be better followed by observing the deformation of the water column profile. This deformation can be characterized by the posi-

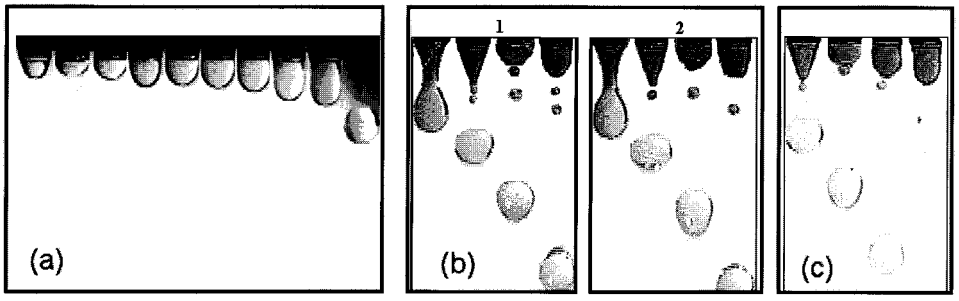

FIG. 3. (a) A drop growing at $f = 1.49$ drops/s showing an oscillatory character. (b) The growing of two successive drops at $f = 6.21$ drops/s showing the occurrence of satellites drops. (c) A satellite being shot laterally at $f = 6.21$ drops/s.

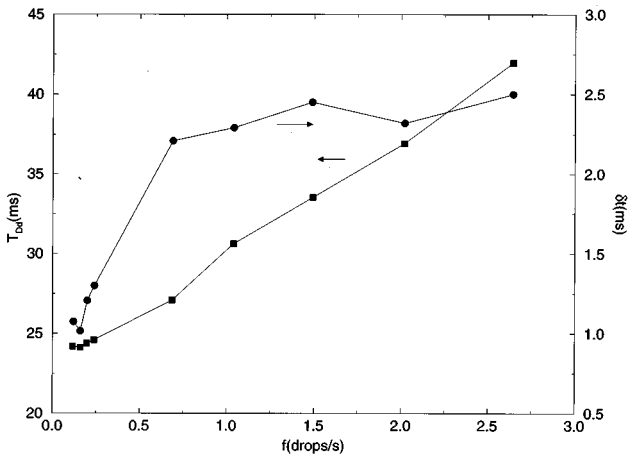

FIG. 4. Time delay (squares) between the main drop and its satellite and the crossing time(circles) of the satellite drop through the laser beam. The continuous lines are guides for the eyes.

tion of the center of mass (y), as shown in Fig. 7(a), where we have the data of three successive drops at $f=1.49$ drops/s and in Fig. 7(b) are shown the data for two successive drops at $f=1.04$ drops/s. In both cases, the center of mass oscillates around a mean straight line ($\langle y(t)\rangle$), with an increasing period, until it reaches a critical region (when the center of mass y_c is close to the nipple radius a) after which the center of mass grows faster, despite the volume continuing to grow linearly with time (see Fig. 6). These results are consistent with the observations made by Watanabe [18] using a high speed camera (500 frames/s) to detect the oscillations of a drop hanging from a tube, thus deriving an expression for the period

$$\tau=4\left(\frac{2\rho}{\sigma\pi}\right)^{1/2}h^{3/2}, \tag{4}$$

where ρ is volumetric density, σ the superficial tension, and h is the drop length defined in the inset of Fig. 1. From the data of Fig. 7 we obtained a reasonable mean value

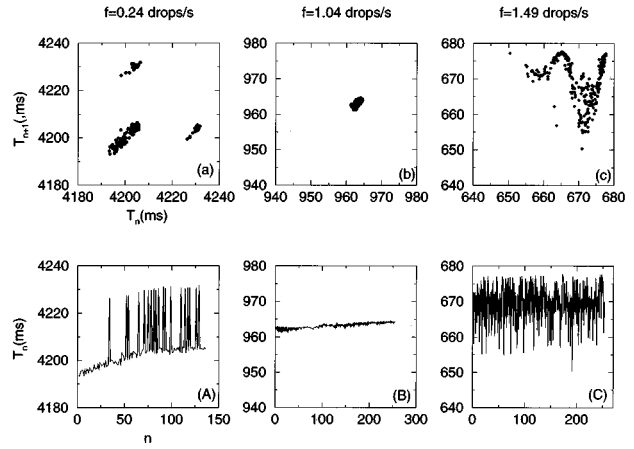

FIG. 5. First return maps T_{n+1} vs T_n in (a), (b), and (c), constructed using only the time between parent drops, (A), (B), and (C), the respective temporal series T_n.

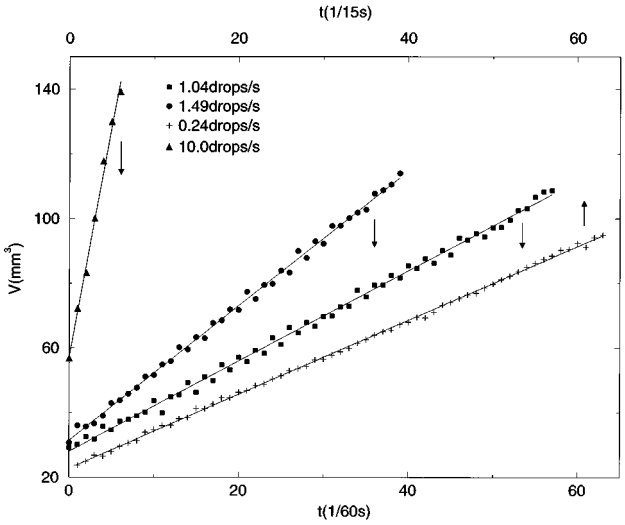

FIG. 6. Volume time evolution for $f=0.24$,1.04,1.49, and 10.0 drops/s. For $f=0.24$ drops/s the digitalization rate was 15 frames/s and 60 frames/s for other drop rates. The continuous lines are the linear fittings of the experimental data.

$\langle\tau\rangle\approx0.07$ s when compared to $\tau=0.09$ s calculated with Eq. (4), taking $\langle h\rangle\approx0.4$ cm and $\sigma=72$ dyn/cm at room temperature.

The motion at $f=1.49$ drops/s shown in Fig. 7(a) is nonperiodic, the successive drops follow the same trajectory only in the linear region and above y_c different trajectories arise, showing a sensibility to the conditions set up when the center of mass is close to y_c. For the case of the periodic motion shown in Fig. 7(b), $f=1.04$ drops/s, the drops follow the same trajectory.

Therefore below y_c the mean behavior of the center of mass is given by a straight line

$$\langle y\rangle=\langle y_o\rangle+\langle v\rangle t, \tag{5}$$

where $\langle v\rangle$ is the mean speed of the center of mass. The water

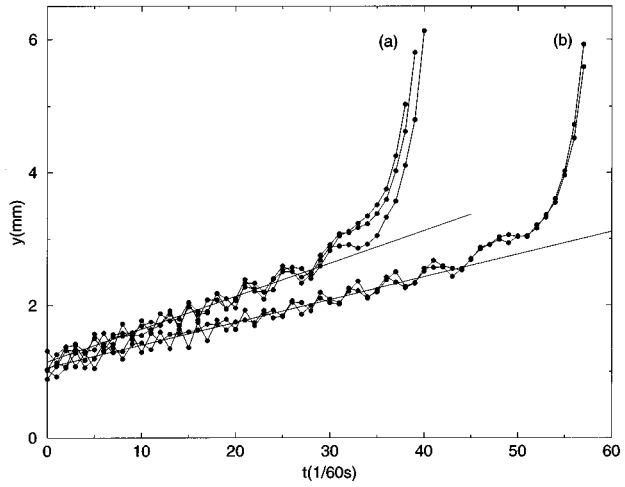

FIG. 7. Time evolution of the center of mass. In (a) we have a nonperiodic motion at $f=1.49$ drops/s while in (b) the motion is periodic at $f=1.04$ drops/s.

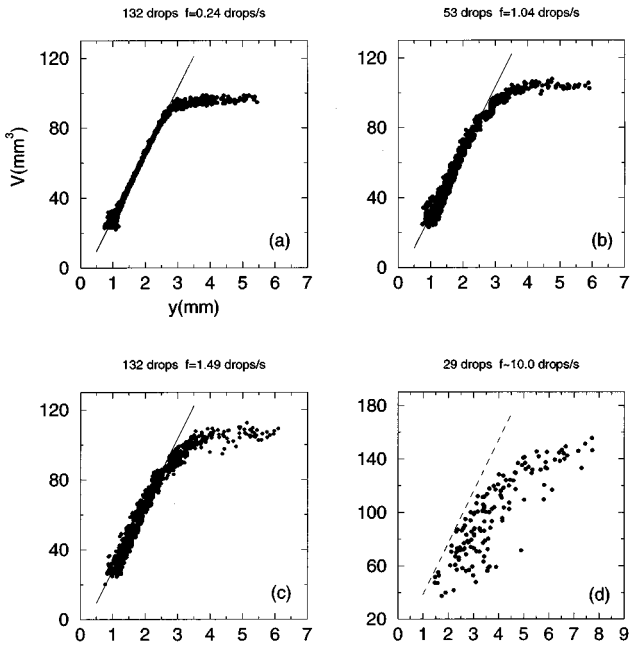

FIG. 8. Volume as a function of the center of mass. The drop rate and the number of drops are indicated in the draws. The images were digitized at 15 frames/s. The continuous lines are the fitting to the quasilinear region. The dashed line was drawn using Eq. (8).

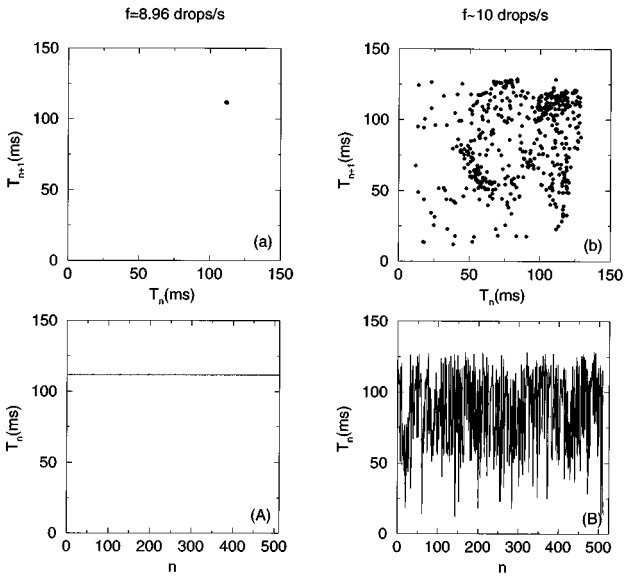

FIG. 9. First return maps T_{n+1} vs T_n in (a) and (b), constructed with 512 data (parent and satellites drops). In (A) and (B) the respective temporal series T_n.

column profile is approximately a cylinder ended by a half-sphere of radius **a** whose volume is given by

$$V \approx \pi a^2 (h - a/3), \tag{6}$$

where a is defined in the inset of Fig. 1. The mean center of mass $\langle y \rangle$ is approximately proportional to $h/2$, therefore a straight line

$$\langle V \rangle = B + C \langle y \rangle \tag{7}$$

fitted to the linear region should give us

$$C = 2\pi a^2 = 38.6 \pm 0.9 \ \text{mm}^2. \tag{8}$$

In Fig. 8 are shown the volume as a function of the center of mass together with the fittings of Eq. (7), for $f = 0.24$, 1.04, 1.49, and 10.0 drops/s, where we have collapsed the data of 132, 53, 132, and 29 successive drops, respectively. In the critical region starts the struggling of the water column, so an elastic limit around $y_c \approx 2.5$ mm is observed. Below y_c the system is elastic and obeys Hook's law, beyond y_c a plastic behavior takes place.

The parameters obtained from the fitting of Eqs. (3), (5), and (7) to their respective linear region are shown in Table I. A good agreement of the C values is achieved when compared to the calculated geometrical value (38.6 mm^2) given by Eq. (8).

The spring constant of Shaw's model [2] can be estimated observing that

$dm/dt \approx \rho \langle \Phi \rangle$, $\langle v \rangle = d\langle y \rangle / dt \approx \langle \Phi \rangle / C$ and with Eqs. (3) and (7) the mean center of mass will be given by

$$\langle y \rangle = \frac{V_o - B}{C} + \frac{\rho g \langle v \rangle C}{k} t \tag{9}$$

by comparison of Eqs. (9) with (5) we have $k = \rho g C$, therefore from data of the fifth column of Table I, $\langle k \rangle \approx 365$ dyn/cm is obtained.

For a higher drop rate the VHS time resolution (1/60 s maximum) does not allow us to obtain enough data for a good characterization of the time evolution of a particular drop. Nevertheless, we follow the growing of ten successive drops in a periodic regimen at $f = 8.96$ drops/s, and 27–29 drops in a nonperiodic regime $f \approx 10$ drops/s. The first return maps, as well as the respective time series, are shown in Fig. 9. For the periodic motion shown no satellites drops were observed among the 512 drops collected. In Fig. 10 are

TABLE I. In the second and third columns are the parameter values obtained from the fitting of Eq. (3) to the linear data V vs y shown in Fig. 8. The values between braces are the results obtained directly from the fitting of Eq. (5).

f (drops/s)	V_o (mm^3)	$\langle \Phi \rangle$ (mm^3/s)	B (mm^3)	C (mm^2)	$\frac{V_o - B}{C}$ (mm) $\{=\langle y_o \rangle\}$	$\frac{\langle \Phi \rangle}{C}$ (mm/s) $\{=\langle v \rangle\}$
0.24	24.0	17.1	-9.1	37.3	0.89	-
1.04	28.1	83.5	-7.3	37.0	0.96 {1.04}	2.26{2.05}
1.49	31.4	124.8	-9.5	37.7	1.08 {1.15}	3.31{2.96}

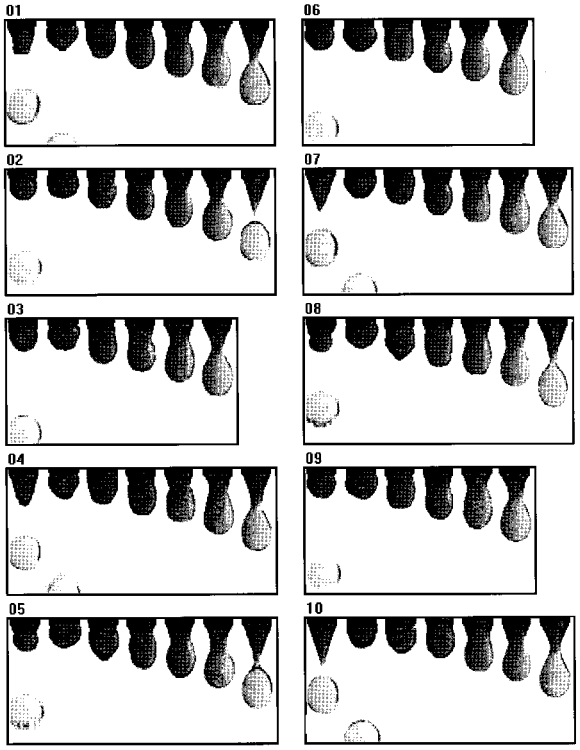

FIG. 10. Images of the formation of ten successive drops at $f = 8.94$ drops/s in a periodic motion.

shown the images of the growing of ten of these drops. For the case of the nonperiodic regime, the dynamics presents a very complex behavior as shown in a sequence of images drawn in Figs. 11–13, but pattern repetition or stationarity [10] can be observed in the sequences of boxes 15–18 and

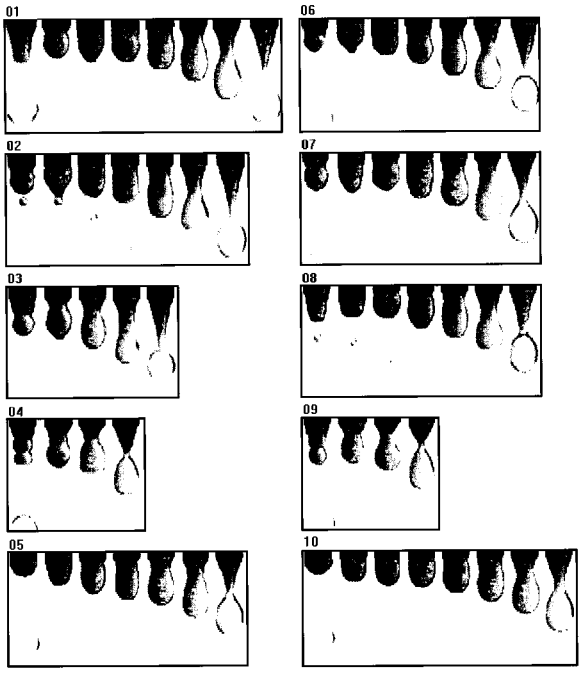

FIG. 11. The first ten boxes of frames of images of the drop growing at $f \approx 10$ drops/s. In the boxes 2 and 8 small satellites drops can be observed.

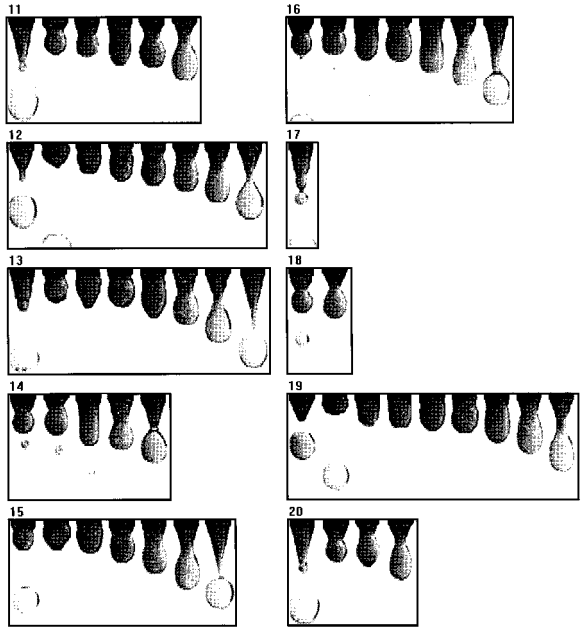

FIG. 12. The sequence of Fig. 11. In boxes 14 and 16 small satellites drops can be observed, and in boxes 17 and 18 big ones.

25–28. The drop time formation can be as short as 50 ms or as long as 134 ms. Sometimes the formation of small satellite drops occurs, boxes 2,8,14,16, and 24 in Figs. 11–13, as well as the formation of big satellites drops, boxes 17,18,27, and 28 in Figs. 11 and 13. As the laser data acquisition system detects all the drops, the presence of satellites drops makes it more difficult to calculate the drop rate, once if we took them into account we would obtain values not compatible with the

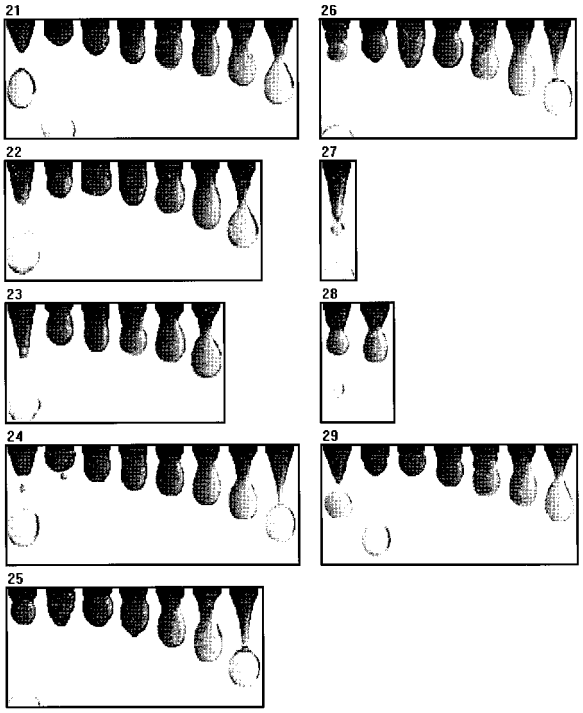

FIG. 13. The sequence of Fig. 12. Small satellite drops are shown in box 24 and big satellites drops are observed in boxes 27 and 28.

time formation of the parent drop. Therefore the value $f \approx 10$ drops/s was obtained taking off 92 satellites drops ($T_n < 10$ ms) from a file of 512 drops.

IV. CONCLUSION

The dynamics of the water drop formation can be divided into two parts. Firstly, the mean behavior of the volume and center of mass can be explained by the spring-mass system proposed by Shaw (elastic behavior); secondly, a nonlinear dynamics (plastic behavior) of the water formation, that seems to start with the struggling of the water column in the nipple faucet, with sensibility to the initial conditions set up at a critical point y_c. The appearance of satellite drop following every parent drop can lead to a misinterpretation of the attractor when we construct first returns maps for low drop rates. In such cases we found that the best procedure is to add up the satellite and its parent drop data.

This work was partially financed by Finep, CNPQ, and Fapesp.

[1] P. Martien, S. C. Pope, P. L. Scott, and R. S. Shaw, Phys. Lett. **110A**, 339 (1985).
[2] R. Shaw, *The Dripping Faucet as a Model Chaotic System* (Aerial, Santa Cruz, CA, 1984).
[3] H. N. N. Yépez, A. L. S. Brito, C. A. Vargas, and L. A. Vicente, Eur. J. Phys. **10**, 99 (1989).
[4] R. F. Cahalan, H. Leider-her, and G. D. Cahalan, Comput. Phys. **4**, 368 (1990).
[5] X. Wu and Z. A. Schelly, Physica D **40**, 433 (1989).
[6] K. Dreyer and F. R. Hickey, Am. J. Phys. **59**, 619 (1991).
[7] J. C. Sartorelli, W. M. Gonçalves, and R. Pinto, Phys. Rev. E **49**, 3963 (1994).
[8] R. D. Pinto, W. M. Gonçalves, J. C. Sartorelli, and M. J. de Oliveira, Phys. Rev. E **52**, 6896 (1995).
[9] T. J. P. Penna, P. M. C. de Oliveira, J. C. Sartorelli, W. M. Gonçalves, and R. D. Pinto, Phys. Rev. E **52**, R2168 (1995).
[10] X. D. Shi, M. P. Brenner, and S. R. Nagel, Science **265**, 219 (1994).
[11] S. D. R. Wilson, J. Fluid Mech. **190**, 561 (1988).
[12] D. H. Peregrine, G. Shoker, and A. Symon, J. Fluid Mech. **212,** 25 (1990).
[13] D. W. DePaoli, J. Q. Feng, O. A. Basaran, and T. C. Scott, Phys. Fluids **7**, 1181 (1995).
[14] X. Zhang and O. A. Basaran, Phys. Fluids **7**, 1184 (1995).
[15] A. Laverón-Simavilla and J. M. Perales, Phys. Fluids **7**, 1204 (1995).
[16] G. I. Sánches-Ortiz and A. L. Salas-Brito, Phys. Lett. A **203**, 300 (1995); G. I. Sánches-Ortiz and A. L. Salas-Brito, Physica D **89**, 151 (1995).
[17] P. M. C. de Oliveira and T. J. P. Penna, J. Stat. Phys. **73**, 789 (1993). P. M. C. de Oliveira and T. J. P. Penna, Int. J. Mod. Phys. C **5**, 997 (1994).
[18] Y. Watanabe, Jpn. J. Appl. Phys. **24**, 351 (1985).